Research Paper

Catalytic oxidation of 2-(methylthio)-benzothiazole on alkaline earth titanates, ATiO$_3$ (A = Ca, Sr, Ba)

Daniela A. Salinas [a,c,*], Candelaria Leal Marchena [b,*], Liliana B. Pierella [b], Gina Pecchi [c]

[a] Department of Chemistry, University of Bío-Bío. Concepción, Chile
[b] Centro de Investigación y Tecnología Química (CITeQ), UTN-CONICET. MAestro López esq. Cruz Roja Argentina. 5016. Córdoba, Argentina
[c] Department of Physical Chemistry. University of Concepción. Concepción, Chile

ABSTRACT

The effect of the nature of the A-cation in alkaline earth titanates, ATiO$_3$ (A = Ca, Sr, Ba), and the calcination temperature (600 °C, 700 °C) on the catalytic performance for the oxidation of 2-(methylthio)-benzothiazole is reported. The solids were characterized by nitrogen adsorption isotherms, powder X-ray diffraction, O$_2$ temperature-programmed desorption, temperature-programmed reduction, Fourier transform infrared spectroscopy, and diffuse reflectance spectroscopy/UV–vis techniques. A larger extent of the perovskite-type structure was obtained for the alkaline earth titanates at a calcination temperature of 700 °C. The increases in the catalytic oxidation with the ionic ratio of the A-cation (BaTiO$_3$ > SrTiO$_3$ > CaTiO$_3$) was attributed to the well-defined perovskite structure with a lower extent of segregated phases. For the catalysts calcined at 700 °C, a larger conversion level (>75 mol%) and selectivity towards the corresponding sulfone (>95 mol%) was achieved at a reaction temperature of 60 °C using H$_2$O$_2$ (30%) as an oxidant. BaTiO$_3$ calcined at 700 °C, provided the better catalytic performance and no activity loss after four reuses, indicative of the largest stability in the reaction medium.

© 2017 Elsevier B.V. All rights reserved.

1. Introduction

Benzothiazoles are organosulfur compounds that have a variety applications, including pharmacological activity, agricultural uses [1,2], stabilizers in the photo industry [3], and corrosion inhibitors in dishwater detergents and de-icing/anti-icing fluids [4]. Benzothiazoles have been considered as emerging contaminants in industrial wastewater, which are released from rubber products, released from pharmacology production plants as effluents, or leached from the fine particles of automobile tires [5,6], and can be oxidized to the respective sulfoxide or sulfone. Benzothiazole removal of up to 70% can be obtained in conventional sewage plants [7] and by the activated sludge treatment process [8]. Recently, the selective oxidation of sulfide to the corresponding sulfone has received much attention in commodities for the biological and pharmaceutical industries [9–11] and to obtain more biodegradable compounds [12,13]. A larger selectivity towards the sulfoxide can be achieved at lower temperatures (~25 °C), and higher temperatures increase the selectivity towards the sulfone [14], which is

used as a synthetic intermediate [15]. Sulfones can also be obtained from sulfide oxidation by employing strong oxidants [16]. H$_2$CrO$_4$ [17], NaBO$_3$ [18], molecular oxygen [19], hydrogen peroxide [20], and tert-butyl hydroperoxide [21] have been reported as oxidants. A reaction scheme is propose in Scheme 1. Catalytic sulfide oxidation with H$_2$O$_2$ is an environmentally friendly process [22]. However, to obtain a large conversion level and selectivity towards sulfone, elevated temperatures and long reaction times are necessary [14]. Thus, new highly selective heterogeneous catalysts are required for mild reaction conditions. Earth titanates mixed with a perovskite structure, ATiO$_3$ (A = Ca, Sr, Ba), have been reported as effective catalysts for photo oxidation because the stabilization of different oxidation numbers of the B-cation allows for visible light absorption [23–25]. For oxidation reactions, their catalytic activity was correlated to vacancies and the formation of structural defects [26,27]. Moreover, the reported benefits of reuse of perovskite-type structures [28] is an additional contribution to the principles of green chemistry. In this manuscript, we report the effect of the nature of the A-cation (ATiO$_3$; A = Ca, Sr, Ba), calcination temperature (600 °C and 700 °C), and reuses in the catalytic performance of 2-(methylthio)-benzothiazole oxidation.

* Corresponding authors.
   E-mail addresses: dasalinas@udec.cl (D.A. Salinas), cleal@frc.utn.edu.ar (C.L. Marchena).
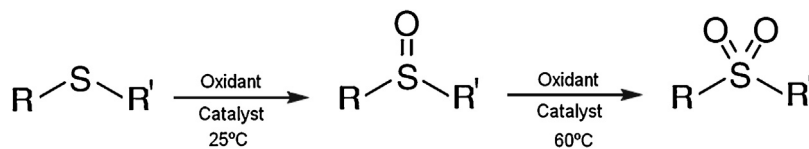
Scheme 1. Selective oxidation de sulfide to sulfoxide and/or sulfone.
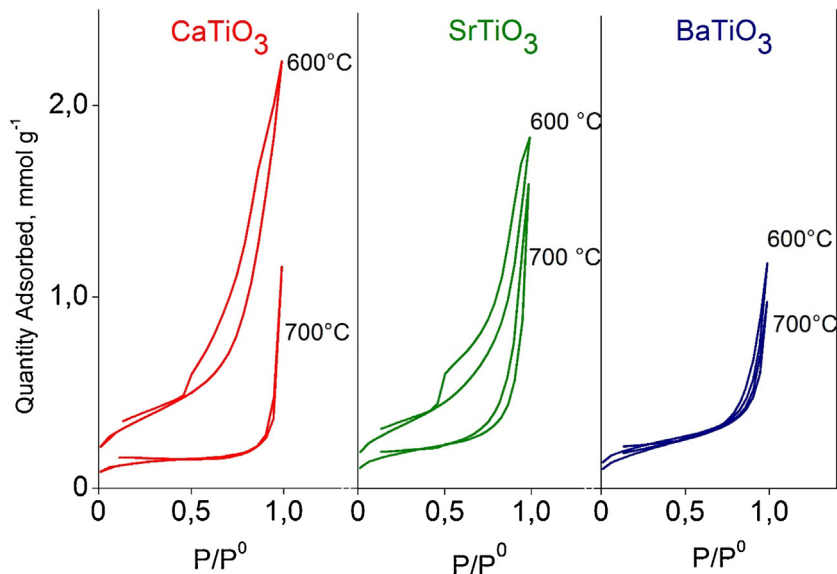
Fig. 1. N$_2$ adsorption-desorption isotherms of CaTiO$_3$, SrTiO$_3$, and BaTiO$_3$ calcined at 600 °C and 700 °C.

2. Experimental

2.1. Preparation of the catalysts

The alkaline earth titanates, CaTiO$_3$, SrTiO$_3$, and BaTiO$_3$, were prepared by the polymerized complex method [29]. Tetraethyl-orthotitanate was used as a titanium precursor, and the respective nitrates were used as alkaline earth metal precursors. Ammonium citrate ((NH$_4$)$_2$C$_6$H$_6$O$_7$) dissolution was used as a complexing agent (10% in excess to guarantee metal-complex formation). The nitrate precursors were dissolved by shaking with citrate at a constant stir rate and precipitated in methanol to produce the A-Ti[C$_3$H$_6$O)(COO)$_3$]$_2$ (A = Ca, Sr, Ba) precursor. The precipitate was filtered and washed with several portions of methanol followed by vacuum drying for 10 h and a calcination procedure in air at 600 °C or 700 °C for 9 h (1 °C min^{-1}).

2.2. Characterization

The Brunauer-Emmett-Teller (BET) specific surface areas (S$_{BET}$) and pore volumes of the perovskites were determined from nitrogen sorption measurements at 77 K using a Tri Star II 3020 instrument. Prior to the measurements, the samples were outgassed at 300 °C for 2 h. The total pore volume (Vp) was recorded by nitrogen adsorption at a relative pressure of 0.99. Powder X-ray diffraction (XRD) spectra were obtained using a D4 Endeavor Bruker AXS diffractometer equipped with nickel-filtered CuKα1 radiation (λ = 1.5418 Å). The standard scan parameters were 2° min^{-1} for the 2θ range from 20 to 90°. The phases were identified by comparing the diffraction patterns to the reference diffraction files in the EVA software. For the O$_2$ temperature-programmed desorption (TPD) experiments, the samples were preheated in an O$_2$ flow for 1 h at 700 °C, cooled to room temperature in the same atmosphere, and then switched to a helium flow with the oxygen desorption monitored using a thermal-conductivity detector, TCD. Temperature-programmed reduction (TPR) was carried out using a Micromeritics TPR/TPD 2900 system equipped with a TCD detector. In the experiment, 0.050 g of the sample was heated from 25 °C to 850 °C at 10 °C min^{-1} under a 5% H$_2$/Ar flow at 50 mL min^{-1}. The FTIR spectra were recorded between 4000 cm^{-1} and 500 cm^{-1}. The IR measurements were performed using a Nicolet Nexus FTIR spectrometer, and the spectra were recorded with 4 cm^{-1} resolution and 250 scans. The diffuse reflectance spectra (DRS) of the materials were recorded using a UV–vis JASCO V 650 spectrophotometer (a diffuse reflectance chamber with an integrating sphere (60 mm diameter) and internal Spectralon coating was attached to this spectrophotometer) in the 200–800 nm wavelength range.

2.3. Catalytic test

2-(Methylthio)-benzothiazole (2-MTBT, 97%, Aldrich; 2 mmol) and 100 mg of a catalyst in acetonitrile (99.5%, Cicarelli, 6 mL) were added to 20 mmol of H$_2$O$_2$ (30 wt%, Cicarelli). The mixture was stirred with a magnetic stirrer (to suppress external mass transfer limitations) and immersed in a thermostated bath equipped with a reflux condenser. The catalytic tests were performed at 60 °C for 60 min, and the conversion of 2-MTBT was monitored by taking aliquots of the reaction mixture at different reaction times. Prior to analysis, the catalyst was separated by filtration and the reaction was analyzed in a Perkin Elmer 500 gas chromatograph (GC) equipped with a capillary column (ZB-1), flame ionization detector (FID), and Shimadzu QP 5050 GC–17 A GC/mass spectrometer (MS) using an HP-5 (25 m × 0.2 mm i.d.) capillary column.

2.4. Reuse catalytic test

For the reuse experience, after a catalytic evaluation the catalysts were separated from the liquid phase, washed with
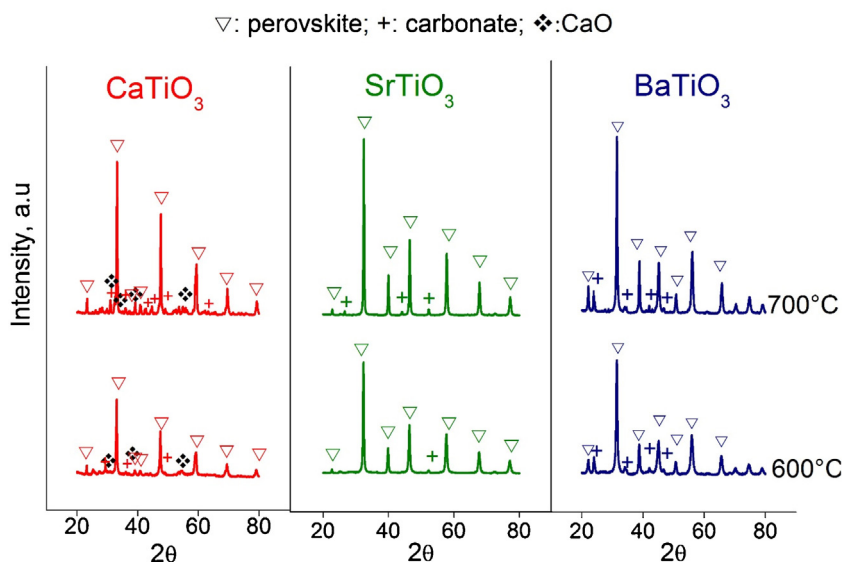
▽: perovskite; +: carbonate; ❖:CaO

Fig. 2. XRD patterns of CaTiO₃, SrTiO₃, and BaTiO₃ calcined at 600 °C and 700 °C.
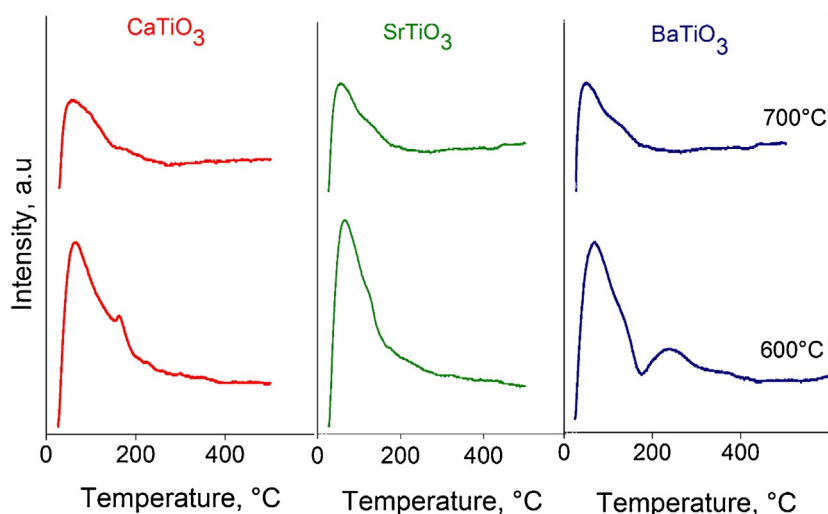
Fig. 3. Oxygen desorption temperatures of CaTiO₃, SrTiO₃, and BaTiO₃ calcined at 600 °C and 700 °C.

acetonitrile (99.5%, Cicarelli), and submitted to different thermal treatments to evaluate the regeneration procedure for the catalysts. For some experiments, the catalysts were dried under vacuum and were calcined in air at 500 °C. For other experiments, the catalysts were only dried in air at 140 °C for 24 h without a new calcination procedure. The catalysts were reuse following the procedure described in catalytic test.

3. Results and discussion

3.1. Surface area

Fig. 1 shows the nitrogen adsorption-desorption isotherms, and Table 1 compiles the surface area of the alkaline earth titanates at the studied calcination temperatures. The well-defined type IV (IUPAC classification) characteristics of mesoporous materials are seen [30], which are strongly influenced by the nature of the alkaline earth metal. For CaTiO₃ and SrTiO₃, the evident hysteresis loop characteristics of mesoporous materials that appear at 600 °C decrease in intensity for the samples calcined at 700 °C. This is an expected result attributed to the interconnectivity process of the
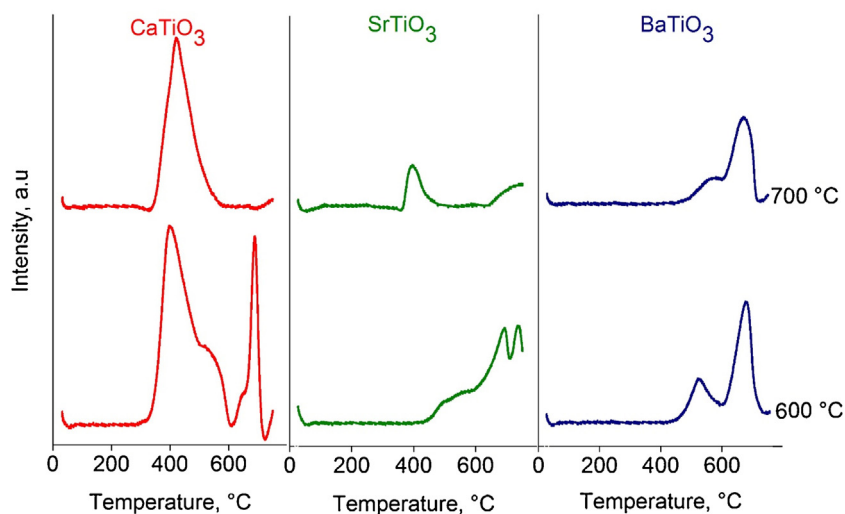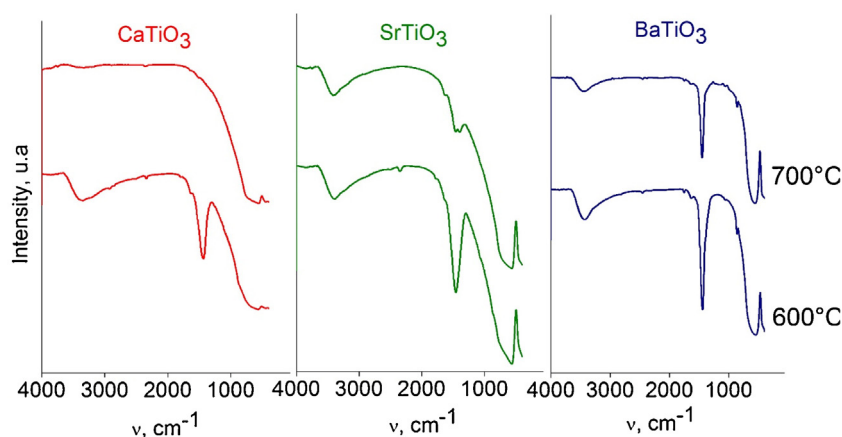
pores with the calcination temperature. A different behavior is seen for BaTiO₃; there are almost no differences in the porosity with respect to the calcination temperature. In Table 1, the observed S_{BET} values indicate larger differences in the surface area based on the calcination temperature for CaTiO₃, followed by SrTiO₃, and almost no effect for BaTiO₃. Therefore, the effect of the calcination temperature (600 °C or 700 °C) on the textural properties of the studied alkaline earth titanates has a larger effect on CaTiO₃ and SrTiO₃ than BaTiO₃.

3.2. X-ray diffraction

The XRD patterns of the alkaline earth titanates with respect the calcination temperature are shown in Fig. 2 and indicate larger differences based on the nature of the alkaline earth metal than the calcination temperature. For CaTiO₃, the diffraction lines at $2\theta = 23°$, 33.3°, 39°, 41°, 47.5°, 59.4°, and 69.5° are attributed to an orthorhombic CaTiO₃ (42-0423) perovskite structure [31–34], the small peak at $2\theta = 24.5°$ is associated with anatase TiO₂ [35], and the peak at $2\theta = 29.45°$ is attributed to CaCO₃ [36,37] and some segregated carbonate phases [37]. No new crystalline phases of

Table 1
Specific area, crystal size, oxygen desorption, hydrogen consumption and band gap energy of $CaTiO_3$, $SrTiO_3$ and $BaTiO_3$ calcined at 600 °C and 700 °C.

Catalyst	S_{BET}, $m^2 g^{-1}$	d_{hkl}, nm	O_2-DTP, mmol O_2 g^{-1}	H_2-TPR, mmol H_2 g^{-1}	E_{gap}, eV
$CaTiO_3$ 600 °C	28	16	2.34	1.19	3.00
$CaTiO_3$ 700 °C	10	25	0.18	0.83	3.50
$SrTiO_3$ 600 °C	25	23	2.18	0.59	3.23
$SrTiO_3$ 700 °C	14	28	0.20	0.19	3.25
$BaTiO_3$ 600 °C	17	46	3.94	0.46	3.30
$BaTiO_3$ 700 °C	15	48	0.33	0.41	3.30

Fig. 4. Hydrogen reduction profiles of $CaTiO_3$, $SrTiO_3$, and $BaTiO_3$ calcined at 600 °C and 700 °C.

Fig. 5. FTIR spectra of $CaTiO_3$, $SrTiO_3$, and $BaTiO_3$ calcined at 600 °C and 700 °C.

$CaTiO_3$ appeared with respect to the calcination temperature, but it became more crystalline at 700 °C [38]. A different behavior can be seen for $SrTiO_3$, where a cubic symmetric $SrTiO_3$ (35-0734) perovskite structure with almost no segregated phases was detected [23,39–42] for the solid calcined at 600 °C. With the increase of the calcination temperature to 700 °C, more crystalline carbonates as segregated phases appear at $2\theta = 25.2°$, 44°, and 52° [43]. The highly symmetric $SrTiO_3$ cubic perovskite structure [44–46] detected for both previously reported calcination temperatures [23] has a thermodynamically stable phase at room temperature. With regard to $BaTiO_3$, the diffraction patterns are very similar with respect to the calcination temperature, as shown in Fig. 2. The diffraction patterns indicate a tetragonal $BaTiO_3$ perovskite structure (83–1880) [47–49] with the presence of carbonates as segregated phases. The absence of splitting in the diffraction peak at $2\theta = 45°$ for $BaTiO_3$

confirms the absence of the cubic phase [47,50] at the studied calcination temperatures (600 °C and 700 °C). Even though the extent of the appearance of carbonates as segregated phases follow the order $CaCO_3 > SrCO_3 > BaCO_3$, the reported stabilities follow the opposite trend, i.e., $BaCO_3$ has the largest stability [51,52]. The lesser effect of the calcination temperature in the diffraction profiles for $SrTiO_3$ and $BaTiO_3$ (Fig. 2) support the easy formation of the perovskite with the increases in the ionic ratio [53] and the high stability of the Ba and Sr [47,50,54,55] carbonates. The highly symmetric cubic perovskite structure does not improve the catalytic activity for combustion reactions [56], and the orthorhombic and rhombohedral structures are the most appropriate perovskite-type oxide structures for their use as catalysts [57]; thus, the different catalytic behavior of the prepared alkaline earth titanates are expect to depend on the nature of the A cation.
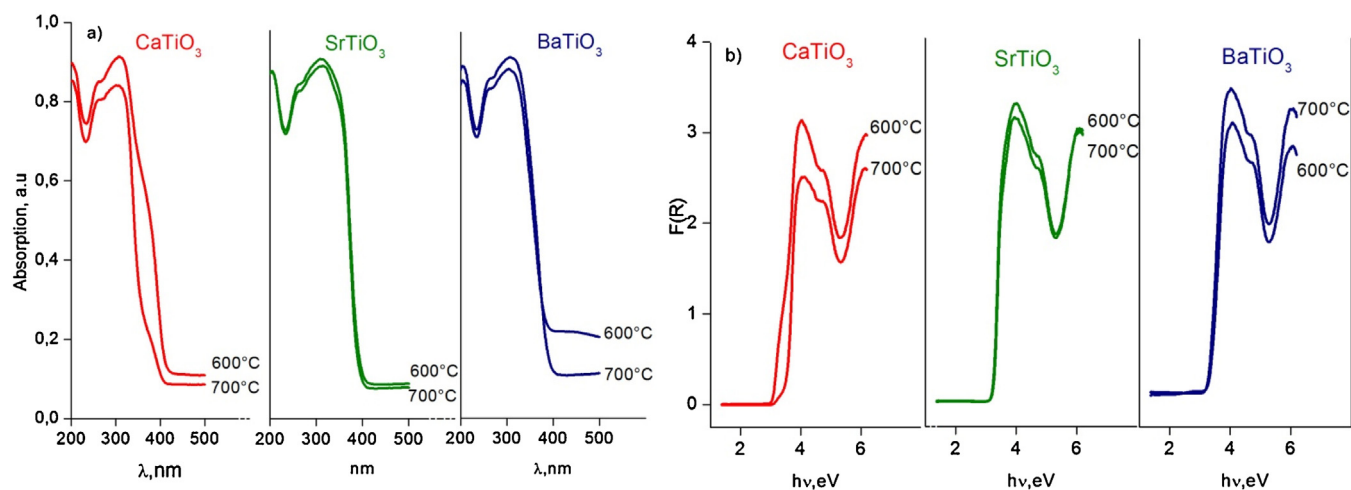
Fig. 6. a) DRS spectra of $CaTiO_3$, $SrTiO_3$, and $BaTiO_3$ calcined at 600 °C and 700 °C; b) Kubelka-Munk function, F (R) and energy [eV].
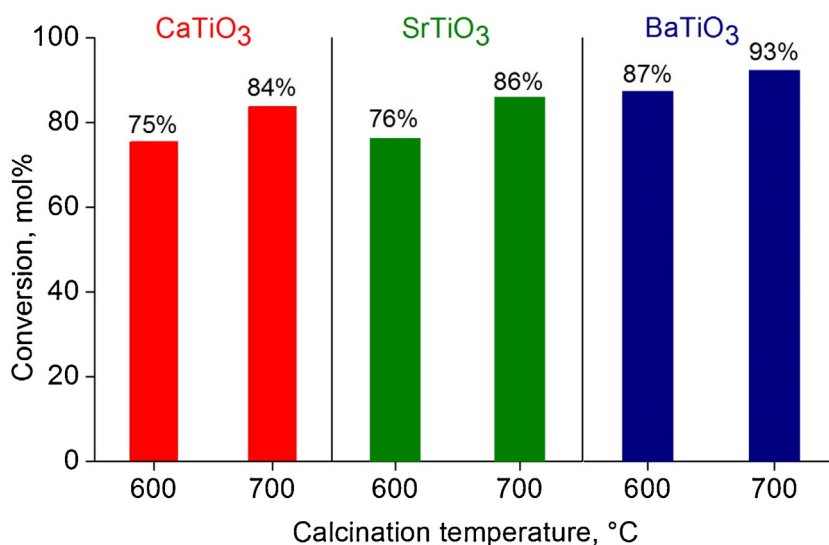

Fig. 7. Conversion of 2-MTBT on $CaTiO_3$, $SrTiO_3$, and $BaTiO_3$ calcined at 600 °C and 700 °C. Reaction conditions: 2-MTBT (2 mmol), oxidant (20 mmol), catalyst (100 mg), acetonitrile (6 mL), 60 °C, 60 min of reaction.

3.3. Temperature-programmed desorption of oxygen (O_2-TPD)

The evolution of oxygen during TPD (Fig. 3) indicates similar desorption profiles for each of the studied alkaline earth titanates. For the perovskite-type oxides, the desorbed oxygen can be related to redox properties [41]. Thus, oxygen desorbed at T < 100 °C corresponds to physically adsorbed oxygen species, the desorption peak in the range of 200 °C < T < 500 °C is attributed to chemically adsorbed oxygen (O^- species), and the latter desorbed oxygens at T > 600 °C is ascribed to lattice oxygen (O^{2-} species) [58–61]. Briefly, in Fig. 3, a large desorption peak at ∼100 °C decreases based on the calcination temperature, and almost no effect is observed based on the nature of the A-cation in the titanate calcined at 700 °C. With regard to the samples calcined at 600 °C a well-defined small desorption peak at 164 °C associated with chemisorbed oxygen can be seen for $CaTiO_3$; this appears as a shoulder for $SrTiO_3$ and $BaTiO_3$. Moreover, a broad peak centered at 240 °C, associated with chemically adsorbed oxygen, is seen only for $BaTiO_3$ at 600 °C. Lattice oxygen is expected to be less important than physically and chemically adsorbed oxygen in reactions that occur at room temperature. The TPD-MS experiments confirm that the evolved gas and He flow only contain oxygen; the deconvolution of the oxy-

gen desorption curves using a Lorentzian line shape allows for the calculation of the desorbed oxygen in the corresponding temperature ranges. The total amount of desorbed O_2, shown in Table 1, indicates a larger dependence on the calcination temperature than the nature of the A-site. The lower desorbed oxygen values for titanate calcined at 700 °C are in line with the large crystallinity of the perovskite structures observed by XRD [62] and comparable to that of the other substituted perovskites [63,64]. With regard to the desorbed oxygen of the titanate calcined at 600 °C, the oxygen desorbed species follow the order $BaTiO_3 > CaTiO_3 > SrTiO_3$; and $BaTiO_3 > SrTiO_3 > CaTiO_3$ for desorbed oxygen of the titanate calcined at 700 °C which is the same order as the decreasing ionic radius Ba^{2+} (0.143 nm) > Sr^{2+} (0.127 nm) > Ca^{2+} (0.106 nm).

3.4. Temperature-programmed reduction (TPR)

The TPR profiles shown in Fig. 4 indicate large differences in the reducibility of the alkaline earth titanates based on the nature of the alkaline earth metal and calcination temperature. In line with previous results, larger differences in the reducibility of $CaTiO_3$ and $SrTiO_3$ than $BaTiO_3$ can be seen with respect to the calcination temperature. For $BaTiO_3$ perovskite calcined at both 600 °C and 700 °C,
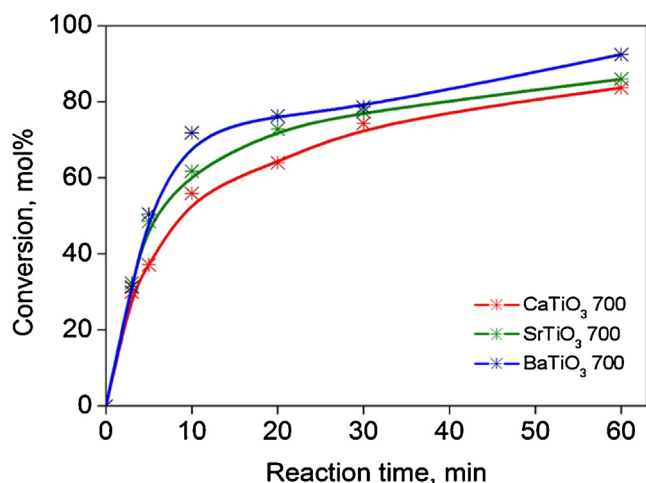
Fig. 8. Conversion of 2-MTBT on $CaTiO_3$ (—＊—), $SrTiO_3$ (—＊—), and $BaTiO_3$ (—＊—) calcined at 700 °C with respect to the reaction time. Reaction conditions: 2-MTBT (2 mmol), oxidant (20 mmol), catalyst (100 mg), acetonitrile (6 mL), 60 °C.

the reduction profiles fit quite well with that of the two reduction processes reported by Li et al. [65]; the first one at 526 °C reported the formation of a perovskite deficiency in O_2 and water [60,66], and the second at 678 °C reported the decomposition of barium carbonates [66]. The decrease in the reduction peak of the non-stoichiometric perovskite structure (526 °C) from 600 °C to 700 °C indicates a greater stability for the large crystalline structure under a reductive atmosphere. The destruction of the $BaTiO_3$ perovskite structure is reported at 800 °C; therefore, it is not detected in the studied temperature range [66]. Large and well-defined reduction peaks are observed for $CaTiO_3$ calcined at both 600 °C and 700 °C, and a narrow reduction peak is observed at 692 °C. The first reduction peak at 403 °C is attributed to the reduction of TiO_2 (Ti^{4+} to Ti^{3+}) in the range of 300–450 °C [67]. Two more reduction peaks are also seen for $CaTiO_3$ at 600 °C: a narrow peak at 692 °C and a broader peak that appears as a shoulder at 544 °C and disappears for $CaTiO_3$ calcined at 700 °C because of the disappearance of segregated phases [36]. The narrowest desorption peak at 692 °C is attributed to reduction of the crystalline CaO phase detected by XRD [68,69]. The absence of this reduction peak for $CaTiO_3$ calcined at 700 °C indicates that this reduction step can start at temperatures >700 °C, and a large reduction temperature is necessary for CaO reduction. For $SrTiO_3$ titanate, the reduction profiles are quite different with respect to the calcination temperatures and indicate different reduction steps. For $SrTiO_3$ calcined at 600 °C, the reduction peaks at 693 °C and 746 °C could be correlated with the decomposition of segregated phases because of carbonate decomposition with the formation of SrO, which is reported at 1300 °C [70]. For $SrTiO_3$ calcined at 700 °C, the reduction peak at 398 °C could be attributed to a partial reduction of Ti^{4+} to Ti^{3+} followed by the formation of the non-stoichiometric perovskite structure. The deconvolution of the reduction profiles using a Lorentzian line shape allows for calculation of the total hydrogen consumption, as shown in Table 1. The larger hydrogen consumption of the alkaline earth titanates calcined at 600 °C is in line with the larger amount and/or easier reduction of the segregated phases detected by XRD.

3.5. Fourier transformed infrared spectroscopy (FTIR)

The infrared spectra of the studied alkaline earth perovskites shown in Fig. 5 agree with the previous characterization results. There is a larger amount of segregated phases for the alkaline earth titanates calcined at 600 °C, and the presence of the characteristic band of the perovskite structure is assigned to stretching of the

Ti—O—Ti bond of the octahedral TiO_6 structure at 857 cm^{-1} [34,60]. With regard to the nature of the A-cation, for $CaTiO_3$ calcined at 600 °C, the band at 3352 cm^{-1} is assigned to the —OH groups of water, and the band at 2337 cm^{-1} is assigned to CO_2 adsorbed on an earth-alkaline metal cation. The carbonate species are detected in the broad band centered at 1440 cm^{-1} [36,71], the signal at 574 cm^{-1} corresponds to a Ca—Ti—O stretching vibration of $CaTiO_3$, and the small band at 863 cm^{-1} corresponds to a O—C—O bending vibration [34,36,72] or Ti—O—Ti bond [34]. For $CaTiO_3$ calcined at 700 °C, the appearance of only the band at 564 cm^{-1} confirms $CaTiO_3$ formation [34,73,74]. For $SrTiO_3$ calcined at 600 °C, the band at 3500 cm^{-1} is associated with —OH groups [75], the small signal at 2347 cm^{-1} is attributed to a CO_2 absorption, and the intense band at 1440 cm^{-1} is associated with carbonate species [76]. A decrease in the intensity of the band for the carbonate species was detected for $SrTiO_3$–700 °C. The similarities for $BaTiO_3$ calcined at 600 °C and 700 °C indicate the presence of —OH groups at 3480 cm^{-1}, CO_2 absorptions on the alkaline earth metal cation at 2452 cm^{-1}, and the presence of CO_3^{2-} species at 1760 cm^{-1} [77]. The signal for $BaTiO_3$ appears at 1450 cm^{-1} and is associated with the asymmetric stretch of the carbonate ion [77], the band at 863 cm^{-1} is associated with the O—C—O bending vibration or Ti—O—Ti bond, and the band at 554 cm^{-1} is assigned to a Ti—O stretching mode.

3.6. Diffuse reflectance spectra (DRS)

The DRS of the alkaline earth perovskites shown in Fig. 6a) clearly show the absorption edge bellow 400 nm, which is attributed to electron transitions from the valence gap by 2p orbitals of oxygen to the conduction band of the empty Ti 3d orbitals [40,78]. The optical bang-gap energies (E_{gap} [eV]) are summarized in Table 1 and were determined by the Kubelka-Munk function, F(R), of the diffuse reflectance spectra (Fig. 6b) and by extrapolating a linear fit of the plot of $F(R) = (1 − R^2)/2R$ as a function of energy [79]. In accordance with the E_{gap} values, the synthesized alkaline earth titanates can be classified as TiO_2 (3.2 eV) semiconductor materials [80] with slight differences based on the nature of the A-cation and calcination temperature. The decrease in E_{gap} for $CaTiO_3$–600 °C compared to that for $CaTiO_3$–700 °C is attributed to the localized gap states induced by reduced Ti^{3+} and oxygen vacancies [80]; almost no changes were observed for $BaTiO_3$, which is in agreement with the previously discussed characterization results.

3.7. Catalytic activity

The catalytic activity, represented as the final conversion (mol%) of 2-MTBT after 60 min of reaction with the alkaline earth titanate catalysts ($CaTiO_3$, $SrTiO_3$, or $BaTiO_3$) calcined at different temperatures (600 °C or 700 °C), is shown in Fig. 7. Even though no significant differences were observed in the 2-MTBT conversion with respect to the calcination temperature (600 °C or 700 °C) and the nature of the A-cation, larger differences were detected for $CaTiO_3$ and $SrTiO_3$ than for $BaTiO_3$. The obtained conversion values (>75 mol%) are larger than those reported when Keggin salts were supported over zeolites [81] and similar to those when transition metal-modified polyoxometalates supported on carbon was employed as catalyst [82]. A comparison of the alkaline earth titanate catalysts and those reported in literature with similar methods including catalytic oxidation of 2-MTBT with H_2O_2 as oxidants, are listed in Table 2.

3.7.1. Effect of the calcination temperature

The largest final conversion level for the alkaline earth titanates calcined at 700 °C shown in Fig. 7 could be the unexpected result because the largest surface area of these catalysts is obtained for the

Table 2
Oxidation of 2-MTBT with CaTiO$_3$, SrTiO$_3$ and BaTiO$_3$ catalysts calcined at 600 °C and 700 °C, and comparison with other catalysts.

Catalyst	Conversion, mol%	Selectivity, mol%		H$_2$O$_2$, mmol	Time, h	Temperature, °C	Reference
		Sulfoxide	Sulfone				
CaTiO$_3$ 600 °C	75	3.9	96.3	20	1	60	_[a]
CaTiO$_3$ 700 °C	84	0.6	98.9	20	1	60	_[a]
SrTiO$_3$ 600 °C	76	2.4	97.5	20	1	60	_[a]
SrTiO$_3$ 700 °C	86	0.6	99.3	20	1	60	_[a]
BaTiO$_3$ 600 °C	87	4.7	95.3	20	1	60	_[a]
BaTiO$_3$ 700 °C	93	1.3	98.7	20	1	60	_[a]
Potassium niobate	99.7	29.7	70.2	20	1	40	[64]
CoW$_{12}$-ZSM-5	99	10	90	19	5	40	[81]
[PW$_{11}$O$_{39}$Ni(H$_2$O)]$^{5-}$ on activated carbon	100	80	20	11	25	40	[91]
H$_4$PMo$_{11}$VO$_{40}$	100	15	85	3	5	25	[92]

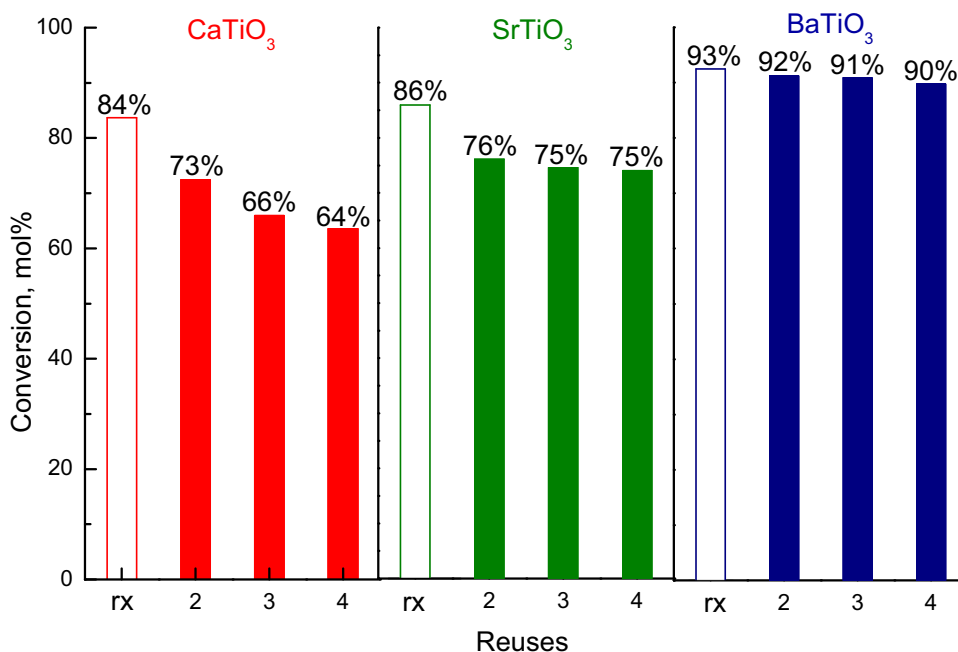[a] Reaction conditions described in the experimental section.
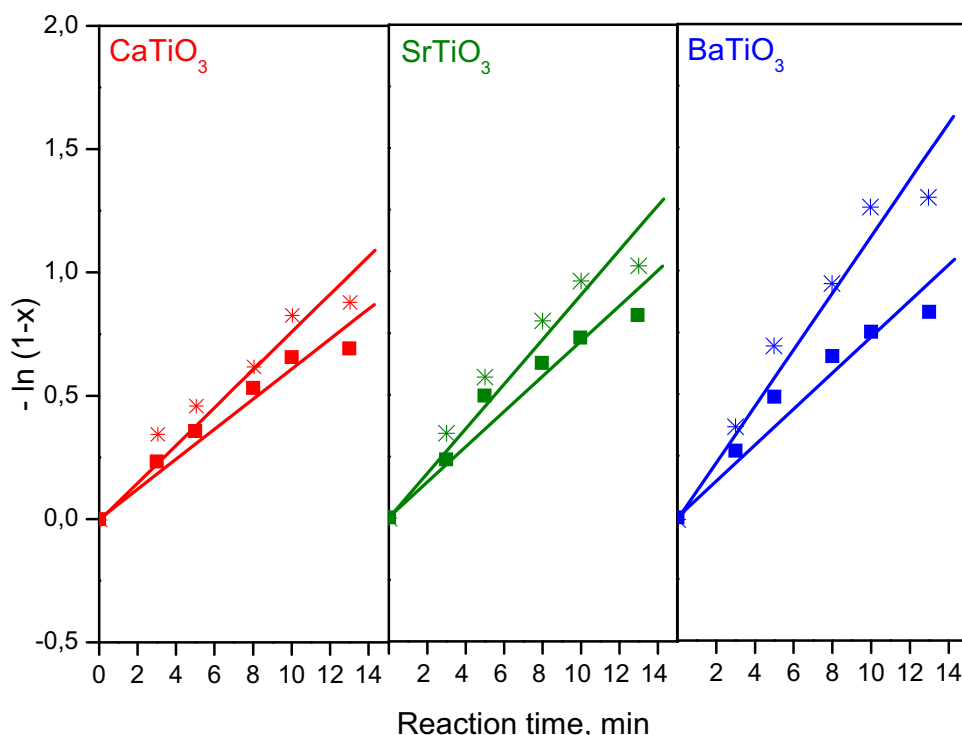
Fig. 9. Pseudo-first-order adjustment of CaTiO$_3$, SrTiO$_3$, and BaTiO$_3$ calcined at (■) 600 °C and (✳) 700 °C.

titanates calcined at 600 °C. Therefore, even though the lowest surface areas were obtained for the CaTiO$_3$–700 °C and SrTiO$_3$–700 °C catalysts, the largest conversion level should be attributed to a well-defined perovskite structure reached at 700 °C, in line with previous reports for the catalytic activity of methane rare-earth perovskite and closely related to the crystalline degree of the perovskite structure [60]. In contrast, the lowest effect of the calcination temperature for BaTiO$_3$ can be explained in terms of the similar surface area and crystalline structure, previously discussed. These results prove the importance of the perovskite structure in the catalytic performance in the 2-MTBT oxidation reaction, which is supported by the lowest reaction rate and pseudo-first-order constant (Table 2) for the perovskite structure with a low crystalline degree and the presence of segregated phases. Thus, even though the largest surface area was obtained for CaTiO$_3$–600 °C, the larger extent of segregated phases and reduced crystalline perovskite structure explains their lower catalytic performances. With regard to BaTiO$_3$, the similar reaction rate seen in Table 3 with respect to the calcination temperature is attributed to its highly stable crystalline structure, larger α-oxygen content, and the stability of the segregated carbonate species with no effect of the

Table 3
Global pseudo first order constant and initial reaction rate of CaTiO$_3$, SrTiO$_3$ and BaTiO$_3$ catalysts calcined at 600 °C and 700 °C.

Catalyst	k, min^{-1}	r$_0$, mmol g^{-1} min^{-1}	R^2
CaTiO$_3$ 600 °C	0.061	1.2	0.98
CaTiO$_3$ 700 °C	0.076	1.5	0.98
SrTiO$_3$ 600 °C	0.071	1.4	0.97
SrTiO$_3$ 700 °C	0.090	1.8	0.97
BaTiO$_3$ 600 °C	0.073	1.5	0.97
BaTiO$_3$ 700 °C	0.114	2.2	0.98

surface area. However, SrTiO$_3$–700 °C displays almost the same surface area as that for BaTiO$_3$–700 °C (Table 1), and its lower reaction rate can be attributed to the crystalline structure of the perovskites, as previously discussed. Therefore, the tetragonal perovskite structure of BaTiO$_3$ explains the highest catalytic activity for 2-MTBT oxidation in line with that reported by Busca et al. [83] and Bradha et al. [25] (i.e., that the increased oxygen vacancies generated by structural distortion of the TiO$_6$ octahedra favor the oxidation reactions). The conversion of 2-MTBT as function of reaction time employing titanates calcined at 700 °C is depicted in Fig. 8.

Fig. 10. Reuse cycles of CaTiO₃, SrTiO₃, and BaTiO₃ calcined at 700 °C for 2-MTBT oxidation. Reaction conditions: 2-MTBT (2 mmol), oxidant (20 mmol), catalyst (100 mg), acetonitrile (6 mL), 60 °C, 60 min of reaction.

A similar behavior was observed for titanates calcined at 600 °C (Figure not shown). The satisfactory fit (Fig. 9) of the experimental data with a pseudo first order reaction (R^2 values ranging from 0.97 to 0.98) allows us to calculate the global pseudo-first-order rate constant (k) and initial reaction rate (r_0) (Table 3). Oxidation of benzothiazole is one of the most straightforward methods for the synthesis of sulfoxides and/or sulfones; both molecules are important synthetic intermediates in organic chemistry. Independently, the catalysts achieved selectivity to sulfone that was higher than 95 mol%, and sulfoxide was the only detected secondary product (Table 2). These results are promising when considering that sulfones are more biodegradable that the corresponding benzothiazole [84]. In order to highlight the importance of the catalysts in the benzothiazole oxidation, a reaction without a catalyst was undertaken using 2 mmol of 2-MTBT and 20 mmol of H_2O_2, and the final conversion was only 7.2 mol%.

3.7.2. Effect of the nature of the A-cation

The effect of the nature of the A-cation in the titanates was studied. Fig. 8 shows that the final conversion depends on the atomic number of the A-cation for titanates calcined at 700 °C: CaTiO₃ (84%) < SrTiO₃ (86%) < BaTiO₃ (93%). For the titanates calcined at 600 °C: CaTiO₃ (75%) < SrTiO₃ (76%) < BaTiO₃ (87%).

The correlation of the catalytic activity with the atomic number of the alkaline metal has been previously reported for alkali carbonates and oxides in carbon black oxidation [85,86], sulfide oxidation with alkali niobates [87], and alkali earth metal oxides as electron promoters of CO oxidation [26]. This behavior was attributed mainly to increased surface electron densities of the active sites while increasing the atomic radii that promote electron transfer from the support, increasing the lattice oxygen. Based on the above discussion for alkaline earth metal titanates, the increase of the catalytic activity with increased atomic radii of the A-cation (Ba > Sr > Ca) could be related to the lower S_{BET}, larger crystallite size, presence of α-oxygen, and increased mobility of the lattice oxygen.

3.7.3. Reuses

Because of the well-known catalyst deactivation by the loss of active phases or blockage of active centers by reaction product adsorption [88], successive reuse cycles were performed using the alkaline earth titanates with the largest conversion level, i.e., those calcined at 700 °C. First, the catalysts were separated from the liquid phase, washed with acetonitrile, and submitted to different thermal treatments after the reaction was complete to determine the regeneration procedure for the catalysts. In some experiences, the catalysts were dried under vacuum and calcined in air at 500 °C, and in other only dried in air at 140 °C for 24 h with no new calcination procedure [89]. Almost no differences were observed for the conversion levels of CaTiO₃, SrTiO₃, and BaTiO₃ after the different regeneration procedures were evaluated; thus, the calcination step was not considered, and the regeneration for the following reuses was performed only with the catalysts dried at 140 °C for 24 h. The conversion levels of 2-MTBT at 60 min of reaction for the successive reaction cycles are shown in Fig. 10, and the first catalytic reaction was also included for a better comparison. Large differences are observed based on the nature of the alkaline earth metal, where CaTiO₃ and BaTiO₃ show the highest and lowest catalytic deactivations, respectively. The large deactivation of CaTiO₃ can be correlated with the large presence of calcium carbonate as a segregated phase detected by XRD, which is easier to leach from the first and successive reuses. Therefore, the continuous decrease in the conversion level can be attributed to leaching of the segregated calcium carbonate phase.

The catalytic activity of alkaline carbonates has been reported by Tang and Wang [90]. To corroborate the catalytic activity in benzothiazole oxidation of the carbonates, a reaction was performed under the same reaction conditions employing CaCO₃ as a catalyst. After 60 min of reaction, a final conversion of 22 mol% was obtained. With regard to SrTiO₃, the loss of activity for only the first reuses indicates the high stability of the catalyst; for BaTiO₃, almost no activity loss is seen after the first and subsequent reuses. These results confirm the high stability of the active Ba carbonate sites, in concordance with the characterization results. The characteriza-

tion results indicate that the differences in the catalytic stabilities of the alkaline earth titanates can be closely related to the stability of the perovskite structure and point out the importance of this crystalline structure in the resistance to leaching.

4. Conclusions

The nature of the A-cation (Ca, Sr, Ba) and calcination temperature (600 °C and 700 °C) for alkaline earth metal titanates indicate that the catalytic activity increases with an increase of the atomic ratio, i.e., $CaTiO_3 < SrTiO_3 < BaTiO_3$. The nature of the A-cation can be correlated to the extent of crystallinity of the perovskite-type structure. $CaTiO_3$ has larger surface areas and segregated phases, which reduce the stability of the perovskite structure, whereas the lower extent of segregated phases increases the stability of $SrTiO_3$ with respect to $CaTiO_3$. The high stability of $BaTiO_3$, with almost no structural and catalytic differences for the catalysts calcined at 600 °C and 700 °C and the possibility of four reuses without significant differences in the conversion level is an outstanding property of these $BaTiO_3$ materials.

Acknowledgments

References

[1] Z. Ji, F. Zhou, S. Wei, Bioorg. Med. Chem. Lett. 25 (2015) 4065–4068.
[2] N. Herrera Cano, M.S. Ballari, A.G. López, A.N. Santiago, J. Agric. Food. Chem. 63 (2015) 3681–3686.
[3] A. Wik, G. Dave, Environ. Pollut. 157 (2009) 1–11.
[4] M.D.A.S. Fouda, A. El-Sonbati, S.A. Hassan, Afr. J. Pure Appl. Chem. 7 (2013) 67.
[5] A.G.A.N.S. Thomaidis, A.A. Bletsou, Global Nest J. 14 (2012) 72–79.
[6] C.M. Reddy, J.G. Quinn, Environ. Sci. Technol. 31 (1997) 2847–2853.
[7] A.S. Stasinakis, N.S. Thomaidis, O.S. Arvaniti, A.G. Asimakopoulos, V.G. Samaras, A. Ajibola, D. Mamais, T.D. Lekkas, Sci. Total Environ. 463–464 (2013) 1067–1075.
[8] A.G. Asimakopoulos, A. Ajibola, K. Kannan, N.S. Thomaidis, Sci. Total Environ. 452–453 (2013) 163–171.
[9] E. Wojaczyńska, J. Wojaczyński, Chem. Rev. 110 (2010) 4303–4356.
[10] I. Fernández, N. Khiar, Chem. Rev. 103 (2003) 3651–3706.
[11] K.A. Stingl, S.B. Tsogoeva, Tetrahedron: Asymmetry 21 (2010) 1055–1074.
[12] S. Ahammed, D. Kundu, M.N. Siddiqui, B.C. Ranu, Tetrahedron Lett. 56 (2015) 335–337.
[13] A.A. Mazioti, A.S. Stasinakis, N. Gatidou, N.S. Thomaidis, H.R. Andersen, Chemosphere 131 (2015) 117–123.
[14] R. Frenzel, Á.G. Sathicq, M.N. Blanco, G.P. Romanelli, L.R. Pizzio, J. Mol. Catal. A: Chem. 403 (2015) 27–36.
[15] F. Liu, Z. Fu, Y. Liu, C. Lu, Y. Wu, F. Xie, Z. Ye, X. Zhou, D. Yin, Ind. Eng. Chem. Res. 49 (2010) 2533–2536.
[16] D.A. Alonso, C. Nájera, M. Varea, Tetrahedron Lett. 43 (2002) 3459–3461.
[17] S. Malik, D. Saha, M.H. Mondal, P. Sar, A. Ghosh, K. Mahali, B. Saha, J. Mol. Liq. 225 (2017) 207–216.
[18] D. Habibi, M.A. Zolfigol, M. Safaiee, A. Shamsian, A. Ghorbani-Choghamarani, Catal. Comm. 10 (2009) 1257–1260.
[19] Z. Zhang, Q. Wu, T. Hashiguchi, T. Ishida, H. Murayama, M. Tokunaga, Catal. Comm. 87 (2016) 18–22.
[20] Z.K.K. Kaczorawska, K. Mitka, P. Kowalski, Tetrahedron 61 (2005) 8315–8327.
[21] G.W. Breton, J.D. Fields, P.J. Kropp, Tetrahedron Lett. 36 (1995) 3825–3828.
[22] F. Jalilian, B. Yadollahi, M.R. Farsani, S. Tangestaninejad, H.A. Rudbari, R. Habibi, Catal. Commun. 66 (2015) 107–110.
[23] T. Alammar, I. Hamm, M. Wark, A.-V. Mudring, Appl. Catal. B 178 (2015) 20–28.
[24] B. Zieliñska, E. Borowiak-Palen, R.J. Kalenczuk, Int. J. Hydrogen Energy 33 (2008) 1797–1802.
[25] M. Bradha, T. Vijayaraghavan, S.P. Suriyaraj, R. Selvakumar, A.M. Ashok, J. Rare Earth 33 (2015) 160–167.
[26] K. Yang, Y. Zhang, Y. Li, P. Huang, X. Chen, W. Dai, X. Fu, Appl. Catal. B 183 (2016) 206–215.
[27] M.A. Bañares, Catal.Today 51 (1999) 319–348.
[28] M.A. Peña, J.L.G. Fierro, Chem. Rev. 101 (2001) 1981–2018.
[29] M. Rajendran, M.S. Rao, J. Mater. Res. 12 (1997) 2665–2672.
[30] S.J. Greeg, K.S.W. Sing, Adsorption, surface area and porosity, Academic Press, London, 1982.
[31] D. Wei, Y. Zhou, D. Jia, Y. Wang, Surf. Coat. Technol. 201 (2007) 8715–8722.

[32] J.P. Wiff, V.M. Fuenzalida, J.L. Arias, M.S. Fernandez, Mater. Lett. 61 (2007) 2739–2743.
[33] A. Alzahrani, A. Samokhvalov, J. Lumin. 178 (2016) 430–436.
[34] J.E. Arce, A.E. Arce, Y. Aguilar, L. Yate, S. Moya, C. Rincón, O. Gutiérrez, Ceram. Int. 42 (2016) 10322–10331.
[35] X. Rao, C.L. Chu, Q. Sun, Surf. Coat. Technol. 302 (2016) 117–125.
[36] G. Pecchi, P. Reyes, R. Zamora, C. Campos, L.E. Cadús, B.P. Barbero, Catal. Today 133–135 (2008) 420–427.
[37] X. Li, X. Xu, Q. Zhou, T. Qi, G. Liu, Z. Peng, Y. Cui, J. Li, Int. Refract. Metals Hard Mater. 60 (2016) 82–91.
[38] A. Kawashima, K. Matsubara, K. Honda, Bioresour. Technol. 99 (2008) 3439–3443.
[39] L. Chen, S. Zhang, L. Wang, D. Xue, S. Yin, J. Cryst. Growth 311 (2009) 746–748.
[40] E. García-López, G. Marcì, B. Megna, F. Parisi, L. Armelao, A. Trovarelli, M. Boaro, L. Palmisano, J. Catal. 321 (2015) 13–22.
[41] W.-D. Yang, K.-M. Hung, J. Mater. Sci. 37 (2002) 1337–1342.
[42] B. Białobok, J. Trawczyński, T. Rzadki, W. Miśta, M. Zawadzki, Catal. Today 119 (2007) 278–285.
[43] W.Y. Hernández, M.N. Tsampas, C. Zhao, A. Boreave, F. Bosselet, P. Vernoux, Catal. Today 258 (Part 2) (2015) 525–534.
[44] T. Puangpetch, T. Sreethawong, S. Yoshikawa, S. Chavadej, J. Mol. Catal. A: Chem. 287 (2008) 70–79.
[45] R. Ubic, K. Tolman, K. Chan, N. Lundy, S. Letourneau, W.M. Kriven, J. Alloys Compd. 575 (2013) 239–245.
[46] F.E. López-Suárez, S. Parres-Esclapez, A. Bueno-López, M.J. Illán-Gómez, B. Ura, J. Trawczynski, Appl. Catal. B 93 (2009) 82–89.
[47] S. Fuentes, R.A. Zárate, E. Chávez, P. Muñoz, M. Ayala, R. Espinoza-González, P. Leyton, J. Alloy Compd. 505 (2010) 568–572.
[48] L.A. Patil, D.N. Suryawanshi, I.G. Pathan, D.G. Patil, Sens. Actuators B 195 (2014) 643–650.
[49] G. Alvarez, A. Conde-Gallardo, H. Montiel, R. Zamorano, J. Magn. Magn. Mater. 401 (2016) 196–199.
[50] X. Yang, Z. Ren, G. Xu, C. Chao, S. Jiang, S. Deng, G. Shen, X. Wei, G. Han, Ceram. Int. 40 (2014) 9663–9670.
[51] S.Y. Wu, X.M. Chen, X.Q. Liu, J. Alloys Compd. 453 (2008) 463–469.
[52] Y. Yang, Y. Sun, Y. Jiang, Mater. Chem. Phys. 96 (2006) 234–239.
[53] Y. Monakhova, P. Agulhon, F. Quignard, N. Tanchoux, D. Tichit, Catal. Today 189 (2012) 28–34.
[54] E. Chávez, S. Fuentes, R.A. Zarate, L. Padilla-Campos, J. Mol. Struct. 984 (2010) 131–136.
[55] R.P. Mahajan, K.K. Patankar, M.B. Kothale, S.A. Patil, Bull. Mater. Sci. 23 (2000) 273–279.
[56] N. Escalona, S. Fuentealba, G. Pecchi, Appl. Catal. A 381 (2010) 253–260.
[57] R. Dinamarca, X. Garcia, R. Jimenez, J.L.G. Fierro, G. Pecchi, Mater. Res. Bull. 81 (2016) 134–141.
[58] G. Pecchi, B. Cabrera, E.J. Delgado, X. García, R. Jimenez, Appl. Catal. A 453 (2013) 341–348.
[59] N.A. Merino, B.P. Barbero, P. Grange, L.E. Cadús, J. Catal. 231 (2005) 232–244.
[60] G. Pecchi, C. Campos, O. Peña, Catal. Today 172 (2011) 111–117.
[61] J. Zhu, Z. Zhao, D. Xiao, J. Li, X. Yang, Y. Wu, J. Mol. Catal. A: Chem. 238 (2005) 35–40.
[62] M. Alifanti, J. Kirchnerova, B. Delmon, Appl. Catal. A 245 (2003) 231–244.
[63] J. Niu, J. Deng, W. Liu, L. Zhang, G. Wang, H. Dai, H. He, X. Zi, Catal. Today 126 (2007) 420–429.
[64] C. Saux, C. Leal Marchena, R. Dinamarca, G. Pecchi, L. Pierella, Catal. Comm. 76 (2016) 58–61.
[65] X. Li, Q. Hu, Y. Yang, Y. Wang, F. He, Appl. Catal. A 413–414 (2012) 163–169.
[66] M. Ghelamallah, S. Kacimi, R.I. Fertout, Mater. Lett. 59 (2005) 714–718.
[67] S. Riyapan, Y. Boonyongmaneerat, O. Mekasuwandumrong, P. Praserthdam, J. Panpranot, Catal. Today 245 (2015) 134–138.
[68] K. Zhao, F. He, Z. Huang, G.-q. Wei, A.-q. Zheng, H.-b. Li, Z.-l. Zhao, J. Fuel Chem. Technol. 44 (2016) 680–688.
[69] L. Yu, W. Li, V. Ducarme, C. Mirodatos, G.A. Martin, Appl. Catal. A 175 (1998) 173–179.
[70] K. Omata, N. Nukui, T. Hottai, Y. Showa, M. Yamada, Catal. Comm. 5 (2004) 755–758.
[71] A.V.M. Parinitha, IJLRST 2 (2013) 495–498.
[72] J. Reyes-Gasga, E.L. Martínez-Piñeiro, G. Rodríguez-Álvarez, G.E. Tiznado-Orozco, R. García-García, E.F. Brès, Mater. Sci. Eng. C 33 (2013) 4568–4574.
[73] D. Zhang, C.-l Zhang, P. Zhou, J. Hazard. Mater. 186 (2011) 971–977.
[74] Y. Deng, S. Tang, S. Wu, Solid State Sci. 12 (2010) 339–344.
[75] M.C. Tarun, M.D. McCluskey, J. Appl. Phys. 109 (2011) 063706.
[76] J.R.d.O. Lima, Y.A. Ghani, R.B. da Silva, F.M.C. Batista, R.A. Bini, L.C. Varanda, J.E. de Oliveira, Appl. Catal. A 445–446 (2012) 76–82.
[77] M.d.C.B. López, G. Fourlaris, B. Rand, F.L. Riley, J. Am. Ceram. Soc. 82 (1999) 1777–1786.
[78] K. Maeda, ACS Appl. Mater. Interfaces 6 (2014) 2167–2173.
[79] S. Hussain, S.K. Hasanain, J. Alloy Compd. 688 (Part A) (2016) 1151–1156.
[80] M.M. Khan, S.A. Ansari, D. Pradhan, M.O. Ansari, D.H. Han, J. Lee, M.H. Cho, J. Mater. Chem. 2 (2014) 637–644.
[81] C. Saux, C.L. Marchena, L.R. Pizzio, L.B. Pierella, J. Porous Mater. 23 (2016) 947–956.
[82] S.M. Islam, A.S. Roy, P. Mondal, K. Tuhina, M. Mobarak, J. Mondal, Tetrahedron Lett. 53 (2012) 127–131.
[83] G. Busca, V. Buscaglia, M. Leoni, P. Nanni, Chem. Mater. 6 (1994) 955–961.

[84] A. Kloepfer, M. Jekel, T. Reemtsma, Environ. Sci. Technol. 39 (2005) 3792–3798.
[85] J.P.A. Neeft, M. Makkee, J.A. Moulijn, Fuel 77 (1998) 111–119.
[86] B.R. Stanmore, J.F. Brilhac, P. Gilot, Carbon 39 (2001) 2247–2268.
[87] C. Leal Marchena, C. Saux, R. Dinamarca, G. Pecchi, L. Pierella, RSC Adv. 6 (2016) 102015–102022.
[88] O.P. Taran, S.A. Yashnik, A.B. Ayusheev, A.S. Piskun, R.V. Prihod'ko, Z.R. Ismagilov, V.V. Goncharuk, V.N. Parmon, Appl. Catal. B 140–141 (2013) 506–515.

[89] K. Fajerwerg, H. Debellefontaine, Appl. Catal. B 10 (1996) L229–L235.
[90] J. Tang, J. Wang, Fuel Process. Technol. 142 (2016) 34–41.
[91] R.A. Frenzel, G.P. Romanelli, M.N. Blanco, L.R. Pizzio, J. Chem. Sci. 127 (2015) 123–132.
[92] V. Palermo, Á.G. Sathicq, P.G. Vázquez, G.P. Romanelli, Phosphorus Sulfur Silicon Relat. Elem. 189 (2014) 1423–1432.